ChemComm

COMMUNICATION

View Article Online
View Journal | View Issue

Cite this: *Chem. Commun.*, 2026, **62**, 2238

Received 30th October 2025,
Accepted 22nd December 2025

DOI: 10.1039/d5cc06185g

rsc.li/chemcomm

Highly stable self-assembled nanotubes from a bipyridinium-based amphiphilic pseudopeptide

Alejandro Vila, Valentina Gauci and Arturo Blanco-Gómez *

Herein, we report an amphiphilic pseudopeptide that spontaneously self-assembles into monodisperse cationic nanotubes under physiological conditions. These nanotubes exhibit fast self-assembly, remarkable thermal stability and thermoreversibility. The self-assembly concentration range is exceptionally broad, enabling the formation of stable hydrogels at concentrations above 5 mM while preserving the nanostructure at micromolar levels.

Self-assembled nanotubes (SANTs) constitute a class of nanomaterials that, due to the intrinsic characteristics of their topology, exhibit promising applications in the fields of nanotechnology and biotechnology.[1] Depending on the type of building block used, the properties of SANTs can be modulated, making them adaptable for functions such as catalysis, molecular transport, or sensing.[2–4]

Within the broad family of SANTs, peptide-based nanotubes stand out as a particularly promising class due to their biocompatibility, synthetic accessibility, and functional versatility.[5,6] Among them, those formed by phenylalanine (Phe) have gained significant attention due to their robust and highly ordered self-assembly, driven by multiple non-covalent interactions. This self-organizing capability has led to a wide variety of nanotubes with highlighted properties such as molecular detection, fluorescence, or piezoelectricity.[7–9]

As seen in other peptide-based self-assembled nanostructures, the introduction of stimuli-responsive abiotic groups has been proposed as a highly promising strategy for controlling supramolecular organization or physicochemical properties.[10,11] However, to date, this approach remains largely unexplored in peptide-based SANTs, which would add significant value to the development of smart materials.

In our previous work,[12] we reported a novel pH-responsive pseudopeptide (**1**, Fig. 1A) incorporating a "vermellogen"[13] unit, a cationic bipyridinium moiety with a highly conjugated hydrazone group (pK_a 9), into a hydrophobic triphenylalanine scaffold. This amphiphilic pseudopeptide exhibits remarkable self-assembly behavior, forming stable nanotubes in acidic media (pH 1–6) at concentrations between 5–10 mM and disassembly at higher pH (>7) due to the formation of a zwitterionic species. These dynamic assemblies further enable the formation of biocompatible hydrogels, demonstrating potential for controlled drug delivery applications.

Building upon these promising results, this study aims to fine-tune the self-assembly properties of this type of bipyridinium-based pseudopeptides. To this end, we have designed and synthesized a pseudopeptidic analogue **2** (Fig. 1A), in which the vermellogen unit is modified by incorporating an aromatic moiety but maintaining the same triphenylalanine sequence. This subtle structural modification is expected to influence the resulting molecular interactions and be translated to the macroscale.

Compound **2** (Fig. 1A) was obtained by solid-phase peptide synthesis following the same procedure used for its homolog **1**.[14] Molecular characterization of the compound was performed

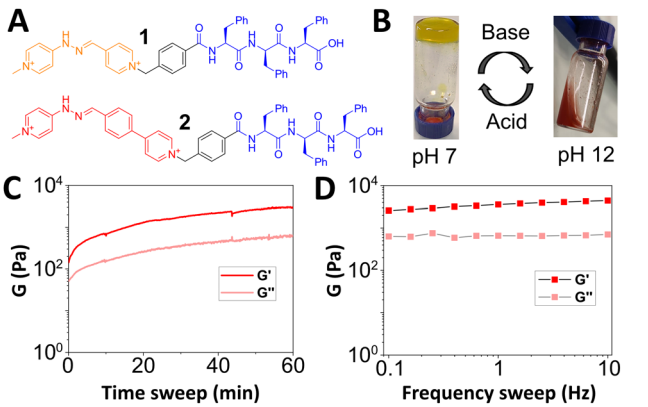

Fig. 1 (A) Chemical structure of **1** and **2**. (B) Pictures of hydrogel obtained at pH 7, and precipitated at pH 12. (C) Time sweep experiment at 1 Pa and 1 Hz at pH 7. (D) Frequency sweep experiment at 1 Pa at pH 7.

Interdisciplinary Center for Chemistry and Biology (CICA) and Department of Chemistry, Faculty of Science, University of Coruña, 15071 A Coruña, Spain. E-mail: arturo.blanco.gomez@udc.es

using 1D/2D NMR, HR-MS and analytical HPLC, confirming the purity and structure of **2**.[14] Similar to **1**, compound **2** contains two ionizable groups within its structure: the carboxylic acid group with a pK_a of 2.9, and the hydrazone group with a value of 10.2.[14] Indeed, the structural modification of the bipyridinium moiety increases the pK_a of the hydrazone group by one unit with respect to the **1** analogue.[12] Furthermore, comparing the HPLC retention times of both compounds, which can be considered an experimental measure of hydrophobicity,[15] **2** (17.3 min) is almost one minute longer than that observed for **1** (16.4 min) under the same elution conditions (Fig. S24, SI).

After molecular characterization of **2**, its self-assembly at high concentrations was evaluated. Within a broad pH range of 1–10 (0.1 M phosphate buffer), where **2** carries at least one net positive charge, it can form hydrogels at concentrations between 5–10 mM (vial inversion test), being faster at neutral pH (30 min) than acidic (>2 h).[14] From pH 10 onwards, the zwitterionic form of **2** precipitates, but the hydrogel can be reversibly recovered upon acidification of the suspension (Fig. 1B). These results indicate that it self-assembles similarly to **1**, forming hydrogels in its cationic state and reversibly disassembling in its zwitterionic form. However, **2** extends the gelation pH range up to 10, exceeding the limit of pH 6 observed for **1**, and therefore can operate within a broader window of physiologically relevant pH values. Therefore, we decided to focus the self-assembly studies at the physiologically more relevant pH of 7.

Dynamic oscillatory rheology confirmed the viscoelastic properties of the hydrogel at 10 mM and pH 7. The time sweep experiment shows fast gelation kinetic, with the elastic modulus (G') being higher than the viscous modulus (G'') since the beginning of the experiment, and reaching stabilization of both at around 60 min (Fig. 1C). The frequency sweep experiment confirms the hydrogel nature, showing G' higher than G'', and both moduli remaining frequency-independent in the range of 0.1–10 Hz (Fig. 1D).

The resulting nanostructure after self-assembly was characterized using transmission electron microscopy (TEM), with negative staining, and small-angle X-ray scattering (SAXS), on the hydrogel at 5 mM. As shown by TEM (Fig. 2A), the pseudopeptide forms nanotubes with micrometer-scale lengths, similar to those observed for **1**.[12] The measured dimensions of the nanotubes (Fig. 2C) show high homogeneity in both outer diameter (27.9 ± 3.1 nm) and wall thickness (4.4 ± 0.5 nm). Moreover, some ribbons were observed in the sample (Fig. 2B), an intermediate structure very common in the formation of SANTs.[16] On the other hand, SAXS data revealed five well-defined oscillations in the range of 0.01–0.1 Å^{-1} (Fig. 3A), consistent with those reported for other self-assembled nanotubes of similar dimensions.[17,18] The data was best fit to a hollow cylinder (HC) model using the SasView software,[14,19] confirming the formation of monodisperse nanotubes. The dimensions of the nanotube obtained from SAXS fitting were 25 nm for the outer diameter and 4.5 nm for the wall thickness, revealing comparable nanotube dimensions between both methods.

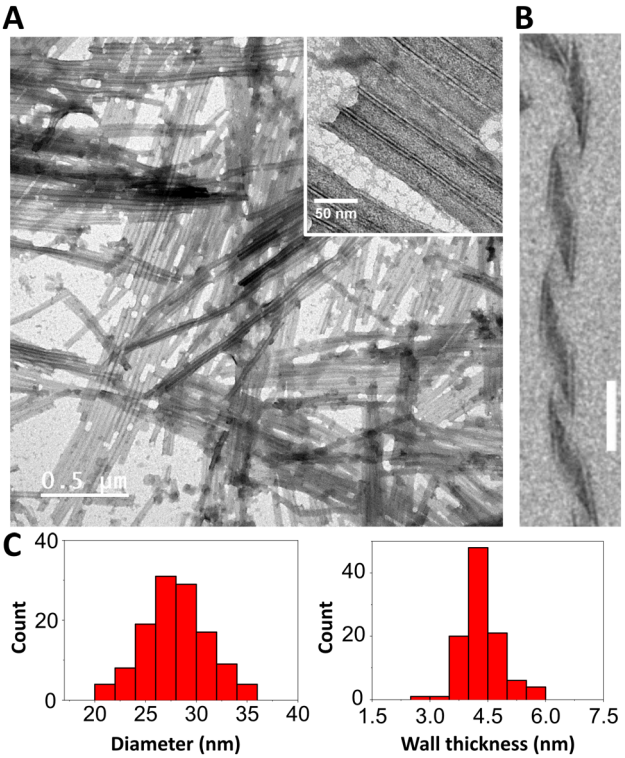

Fig. 2 TEM images of the nanotubes formed by **2** at 5 mM and pH 7 at low (A) and high magnification (inset). (B) TEM image of **2** helical ribbon. Scale bar = 50 nm. (C) Nanotubes diameter (right, n = 120) and thickness (left, n = 120) distributions.

The secondary structure adopted by **2** was characterized using Fourier-transform infrared spectroscopy (FTIR) on the hydrogel prepared in D_2O at pD 7. The amide I region of the FTIR spectrum displayed a main band at 1626 cm^{-1} (Fig. S32, SI), similar to that observed for **1** and, in turn, characteristic of β-sheet secondary structure.[20] Given the parallel β-sheet arrangement in the **1** observed by FTIR and XRD,[12] it is likely that this motif is also favored in the secondary structure of **2**. This arrangement maximizes intermolecular interactions, including C═O···H–N hydrogen bonds (six per molecule) and π–π stacking between the aromatic Phe residues, which are optimally aligned in the same plane.

The self-assembly of **2** was also followed by means of circular dichroism (CD) at 5 mM and pH 7. Similar to its analogue **1**, a bisignet band was observed between 300–450 nm (Fig. 3B), corresponding to the π–π* transitions of the bipyridinium units, characteristic of exciton coupling (EC) band induced by a highly ordered helical arrangement of the chromophores after self-assembly.[21] Unlike its **1** homolog, the kinetics of self-assembly are so fast that the evolution of the EC band cannot be followed over time, in good agreement with the rheological characterization (see above). Additionally, the thermoreversibility of the secondary structure of **2** was investigated over a temperature range of 25–95 °C by monitoring the EC band to determine the melting temperature (T_m). The secondary structure exhibited high stability, retaining 50% of the EC signal even at 95 °C (Fig. 3B). This enhanced stability,

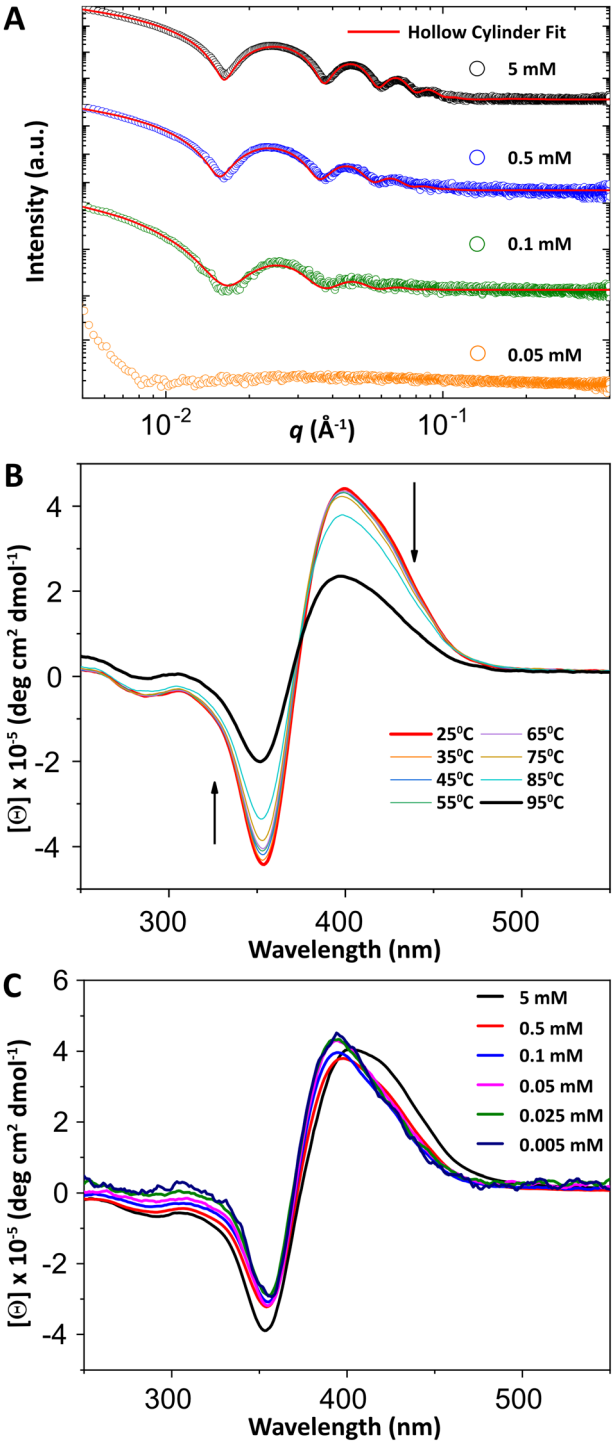

Fig. 3 (A) SAXS data at different self-assembled concentrations of **2** at pH 7 (circles) and the best fits to the HC models (red solid lines). (B) CD spectrum of **2** at 5 mM and pH 7 recorded at different temperatures. (C) CD spectrum of **2** at pH 7 at different concentrations, in the region of the induced EC band.

compared to its shorter analogue **1** (T_m = 85 °C), could be attributed to the above-mentioned higher hydrophobicity observed in the HPLC experiments, as reported for other lipophilic peptides.[22]

Surprised by the remarkable stability of the secondary structure of **2** at pH 7, we carried out a detailed study of its self-assembly and nanotube formation below the critical gelation concentration using CD and SAXS. To avoid kinetic trapping during dilution, solutions of **2** were directly prepared at concentrations ranging from 0.5 to 0.005 mM and equilibrated for 24 hours prior to analysis.

As shown in Fig. 3C, the molar ellipticity [θ] remained constant across the above-mentioned concentration range, even down to 0.005 mM. Below this concentration, further CD measurements were limited by the chromophore's low absorbance. Thermoreversibility studies at 0.1 mM showed a T_m of 56 °C, with complete recovery of the CD signal and nanotube morphology upon cooling to room temperature (Fig. S34–S36, SI). The decrease in T_m compared to the gel state could be attributed to reduced physical entanglement between nanotubes. On the other hand, samples at 0.5 mM and 0.1 mM displayed scattering profiles in SAXS consistent with those observed at 5 mM (Fig. 3A). The SAXS data best fit to an HC model, revealed that nanotube dimensions were largely independent of concentration, with diameters of 26.4 nm (0.5 mM) and 25.2 nm (0.1 mM). At lower concentrations, scattering intensity was insufficient for reliable analysis. However, TEM analysis at 0.05 mM showed nanotubes of similar dimension (Fig. S31, SI), so the formation of nanotubes in solution below 0.1 mM cannot be definitively ruled out. In addition, long-term stability studies at pH 7 and 37 °C showed that the nanotube morphology and associated secondary structure of **2** are preserved for at least three weeks, both in the gel state (5 mM) and below critical gelation concentration (0.1 mM).[14] These results highlight the remarkable stability and self-assembly ability of **2** into nanotubes at micromolar concentrations, significantly surpassing its analogue, which requires a minimum concentration of 1 mM.[12] Notably, this behavior compares favorably with the most peptide- or pseudopeptide-based nanotubes reported to date that are capable of forming nanotubes in aqueous media at high concentration.[23–25] In particular, some Aβ and amphiphilic peptides systems require concentrations in the high micromolar range and often exhibit coexistence of different morphologies,[26–28] whereas only a limited number of systems, such as certain cyclopeptides or peptide-dendron hybrids,[29,30] are known to achieve nanotube formation at lower micromolar concentrations.

Based on our experimental results and previous models of amphiphilic SANT systems,[31] we hypothesize that our nanotubes are formed through a hierarchical self-assembly pathway. The process likely begins with the organization of molecules into a bilayer of alternating β-sheets (Fig. 4A), where phenyl groups orient toward the bilayer core to minimize solvent exposure, while bipyridinium moieties remain exposed. The resulting bilayer thickness model agrees with experimental measurements obtained from TEM and SAXS. Longitudinal growth is directed by C═O···H–N hydrogen bonds and π–π stacking along the β-sheet axis, while electrostatic and van der Waals interactions stabilize lateral lamination. As the bilayer extends, the interplay of these forces may induce curvature, yielding a helical ribbon (Fig. 4B) that eventually closes into a

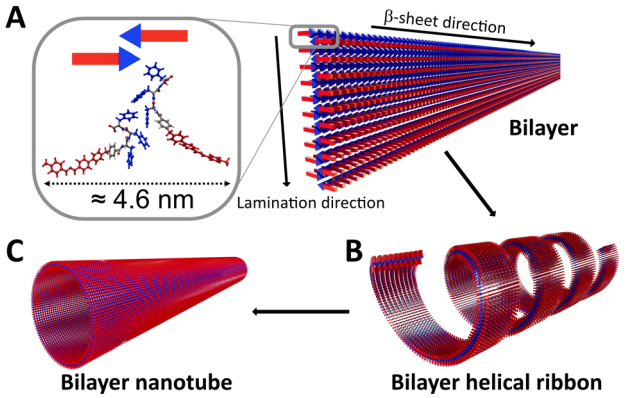

Fig. 4 Schematic representation for the self-assembly mechanism of nanotubes. (A) Illustration of the bilayer self-assembled by alternating β-sheet. Inset: Optimized structures of a **2** dimer,[35] illustrating the bipyridinium unit by a red rectangle and the peptide sequence by a blue triangle. (B) Evolution of the bilayer to the helical ribbon intermediate. (C) Condensation of the helical ribbon intermediate into the bilayer nanotube.

stable bilayer nanotube (Fig. 4C). This pathway is consistent with the helical intermediates observed by TEM and explains the exciton coupling CD signal.

According to the proposed mechanism, the nanotube walls may bear a positive surface charge as a result of the outward exposure of bipyridinium groups. To test this hypothesis, we investigated the interaction between preassembled nanotubes in solution (0.1 mM) and different concentrations of the anionic fluorophore pyranine, which is well known for its fluorescence quenching upon interaction with pyridinium-based molecules.[32] It was observed that, at pyranine concentrations between 10 and 30 μM, fluorescence intensity decreased by more than 87%, with 50% quenching reached at 0.1 mM (Fig. S41, SI). CD studies confirmed that the supramolecular structure of compound **2** remained unaltered under these experimental conditions (Fig. S42, SI). In contrast, no significant changes in fluorescence and CD spectra were detected when using the cationic fluorophore berberine or the neutral Nile Red,[14] both of which are known to modulate their fluorescence in the presence of anionic nanostructures and hydrophobic environments, respectively.[33,34] Overall, the selective interaction with anionic fluorophores suggests the outward orientation of the cationic bipyridinium groups and supports the proposed supramolecular arrangement.

In summary, we report an amphiphilic pseudopeptide that self-assembles in water into stable and monodisperse cationic nanotubes over a broad concentration range. The system forms pH-responsive hydrogels at millimolar concentrations and retains its tubular structure down to the micromolar regime, exhibiting remarkable thermal and structural stability. The outward exposure of bipyridinium groups provides a positive surface charge enabling selective interactions with anionic molecules. These findings highlight the potential of this functional peptide-based scaffolds design to access robust and functional nanostructures suitable for applications in biosensing, supramolecular templates, or molecular compartmentalization.

A.B.-G. thanks the Consellería de Cultura, Educación, e Universidade, Xunta de Galicia for his postdoctoral fellowship (ED481D-2024-020). The authors sincerely thank Professors Marcos D. García and Carlos Peinador for their valuable and unwavering support throughout this work, particularly for their contribution to the computational calculations (M.D.G.) and the illustration (C.P.).

Conflicts of interest

There are no conflicts to declare.

Data availability

The data supporting this article have been included as part of the supplementary information (SI). Supplementary Information: experimental details, synthetic procedures and characterization data, rheological data, TEM analyses, SAXS data, spectroscopic data, computational details. See DOI: https://doi.org/10.1039/d5cc06185g.

References

1 T. Shimizu, W. Ding and N. Kameta, *Chem. Rev.*, 2020, **120**, 2347.
2 H. Zhang, L. Xiong, Z. He, A. Zhong, T. Wang, Y. Xu, M. Zhou and K. Huang, *Polym. Chem.*, 2016, **7**, 4975.
3 H. Xu, S. Nagasaka, N. Kameta, M. Masuda, T. Ito and D. A. Higgins, *Phys. Chem. Chem. Phys.*, 2016, **18**, 16766.
4 Y. Hu, X. Ma, Y. Zhang, Y. Che and J. Zhao, *ACS Sens.*, 2016, **1**, 22.
5 X. Gao and H. Matsui, *Adv. Mater.*, 2005, **17**, 2037.
6 C. Valéry, F. Artzner and M. Paternostre, *Soft Matter*, 2011, **7**, 9583.
7 S. Liu, Y. Luo and G. Liang, *Nanoscale*, 2016, **8**, 766.
8 N. Na, X. Mu, Q. Liu, J. Wen, F. Wang and J. Ouyang, *Chem. Commun.*, 2013, **49**, 10076.
9 J.-H. Lee, K. Heo, K. S.-Schönhagen, J. H. Lee, M. S. Desai, H.-E. Jin and S.-W. Lee, *ACS Nano*, 2018, **12**, 8138.
10 M. E. Rott-Kontforti, M. Comune, M. Halperin-Sternfeld, I. Grigoriants, D. Shabat and L. Adler-Abramovich, *Macromol. Rapid Commun.*, 2018, **39**, 1800588.
11 S. Adorini, G. Goti, L. Rizzo, F. Grassi, S. Kralj, F. Matroodi, M. Natali, R. De Zorzi, S. Marchesan and L. Dell'Amico, *Chem. Commun.*, 2023, **59**, 7619.
12 A. Blanco-Gómez, L. Barravecchia, E. Scarel, R. De Zorzi, L. Colomina-Alfaro, A. Bandiera, S. Kralj, A. Vila, D. Porrelli, C. Peinador, M. D. García and S. Marchesan, *ChemRxiv*, 2025, DOI: 10.26434/chemrxiv-2025-h4vwk.
13 L. Barravecchia, A. Blanco-Gómez, I. Neira, R. Skackauskaite, A. Vila, A. Rey-Rico, C. Peinador and M. D. García, *J. Am. Chem. Soc.*, 2022, **144**, 19127.
14 See SI for further experimental details.
15 H. L. Bolt, C. E. J. Williams, R. V. Brooks, R. N. Zuckermann, S. L. Cobb and E. H. C. Bromley, *Pept. Sci.*, 2017, **108**, e23014.
16 T. G. Barclay, K. Constantopoulos and J. Matisons, *Chem. Rev.*, 2014, **114**, 10217.
17 B. Jean, L. Oss-Ronen, P. Terech and Y. Talmon, *Adv. Mater.*, 2005, **17**, 728.
18 N. Díaz, F.-X. Simon, M. Schmutz, M. Rawiso, G. Decher, J. Jestin and P. J. Mésini, *Angew. Chem., Int. Ed.*, 2005, **44**, 3260.
19 SasView, https://www.sasview.org (accessed 07/2025).
20 H. Yang, S. Yang, J. Kong, A. Dong and S. Yu, *Nat. Protoc.*, 2015, **10**, 382.
21 G. Gottarelli, S. Lena, S. Masiero, S. Pieraccini and G. P. Spada, *Chirality*, 2008, **20**, 471.
22 C. J. Bowerman, D. M. Ryan, D. A. Nissan and B. L. Nilsson, *Mol. BioSyst.*, 2009, **5**, 1058.
23 E. R. da Silva, W. A. Alves, V. Castelletto, M. Reza, J. Roukolainen, R. Hussain and I. W. Hamley, *Chem. Commun.*, 2015, **51**, 11634.

24 Y. Zhao, W. Yang, D. Wang, J. Wang, Z. Li, X. Hu, S. King, S. Rogers, J. R. Lu and H. Xu, *Small*, 2018, **14**, 1703216.
25 X. Ma, Y. Zhao, X. Jiang, M. Fan, C. He, H. Qi, Y. Wang, D. Wang, Y. Ke, H. Xu, C. Chen and J. Wang, *ACS Appl. Mater. Interfaces*, 2024, **16**, 9787.
26 S. Li, A. N. Sidorov, A. K. Mehta, A. J. Bisignano, D. Das, W. S. Childers, E. Schulez, Z. Jiang, T. M. Orlando, K. Berland and D. G. Lynn, *Biochemistry*, 2014, **53**, 4225.
27 V. Castelletto, J. Seitsonen, J. Roukolainen, C. Piras, R. Cramer, C. J. C. Edwards-Gayle and I. W. Hamley, *Chem. Commun.*, 2020, **56**, 11977.
28 K. S. Lee and J. R. Parquette, *Chem. Commun.*, 2015, **51**, 15653.
29 J. Y. Rho, H. Cox, E. D. H. Mansfield, S. H. Ellacott, R. Peltier, J. C. Brendel, M. Hartlieb, T. A. Waigh and S. Perrier, *Nat. Commun.*, 2019, **10**, 4708.
30 H. Shao and J. R. Parquette, *Angew. Chem., Int. Ed.*, 2009, **48**, 2525.
31 T. Shimizu, M. Masuda and H. Minamikawa, *Chem. Rev.*, 2005, **105**, 1401.
32 E. B. de Borba, C. L. C. Amaral, M. J. Politi, R. Villalobos and M. S. Baptista, *Langmuir*, 2000, **16**, 5900.
33 K. Hirakawa, T. Matsuura, Y. Nishimura, H. Mori and S. Takagi, *Photochem. Photobiol. Sci.*, 2025, **24**, 79.
34 D. L. Sackett and J. Wolff, *Anal. Biochem.*, 1987, **167**, 228.
35 The bilayer thickness was determined from a hypothetical structural model of a **2** dimer, derived from the crystallographic conformation of the analogue **1**,[12] modified in its bipyridinium unit and optimized using dispersion-corrected Density Functional Theory methods[14].

